Materials Today Communications 21 (2019) 100648

Contents lists available at ScienceDirect

Materials Today Communications

journal homepage: www.elsevier.com/locate/mtcomm

Density-functional tight-binding approach for the structural analysis and electronic structure of copper hydride metallic nanoparticles

Hasan Kurban[a,b,**], Mustafa Kurban[c,*], Mehmet Dalkılıç[a]

[a] Computer Science Department, Indiana University, Bloomington, 47405, IN, USA
[b] Computer Engineering Department, Siirt University, 56100, Siirt, Turkey
[c] Department of Electronics and Automation, Kırşehir Ahi Evran University, 40100, Kırşehir, Turkey

ARTICLE INFO

Keywords:
Nanoparticles
CuH
Segregation phenomena
Data science

ABSTRACT

We perform a theoretical investigation using the density functional tight-binding (DFTB) approach for the structural analysis and electronic structure of copper hydride (CuH) metallic nanoparticles (NPs) of different size (from 0.7 to 1.6 nm). By increasing the size of CuH NPs, the number of bonds, segregation phenomena and radial distribution function (RDF) of binary Cu-Cu, Cu-H and H−H interactions are analyzed using new implementations in R code. The results reveal that the number of Cu-Cu bonds is more than that of Cu-H while the number of H−H bonds are the less. Thus, a large amount of H atoms prefers to connect to Cu atoms. The increase in the size of the NPs contributes to their stabilization because of the increase in the interaction of H−H bonding. The segregation of Cu and H atoms shows that Cu atoms tend to co-locate at the center, while H atoms tend to reside on the surface. From the density of state (DOS) analysis, CuH NPs shows a metallic character which is compatible with experimental data. HOMO and Fermi levels decrease from -3.555 to -3.443 eV and from -3.510 to -3.441 eV. Herein, an increase in the size contributes to the stabilization of CuH NP due to decrease in the HOMO energies.

1. Introduction

Binary metal hydrides have attracted increasing attention, especially in hydrogen storage applications, due to the ability of metallic atoms to absorb large amounts of hydrogen both safely and efficiently while storing and transporting hydrogen. Among them, copper(ı) hydride (CuH), the oldest hydride known [1], is unique since it can be synthesized in solution at room temperature. Additionally, CuH appears in a myriad of chemical processes, ranging from catalysis to electrochemistry to organic synthesis [2–13]. CuH also exhibits unusual bonding behavior and is unstable at atmospheric hydrogen pressure [14–16], but as a metastable compound, it may be relevant to the applications of copper in which hydrogen entry into the metal is expected.

Elucidating the behavior of nanomaterials is one of the key factors for both science and technology because of their potential unusual properties. One of these curious behaviors is that nanostructures lead to a variety of anomalous phenomena different from their bulk patterns [17–21]. Thus, nanostructured metal hydrides may have the potential to be an important class of materials due to the ability to tune the material properties. In the literature, there has not been any considerable attention paid to CuH material at the nanolevel except for the following two studies: the morphology and stability of CuH nanoparticles (NPs) in different environments [22]. In the study, CuH NPs was found to be very porous and, thus, half the surface area; furthermore, the half-life of CuH may be controlled by the mobility of hydrogen atoms in the copper matrix. CuH nanoclusters have been applied for energy storage and conversion [23]. On the other hand, CuH in wurtzite bulk form exhibits a semiconductor character, whereas, interestingly, CuH at the nanolevel shows metallic character with particle sizes between 44 and 149 μm [22–26].

In this work, for the first time, the structural and electronic properties of CuH NPs have been carried out by a density functional based tight binding (DFTB) method whose run-time complexity is fast and efficient. Moreover, the performance of DFTB calculations has been shown on metallic nanoparticles in the previous studies [27,28]. In this study, we analyzed the HOMO, LUMO and the frontier molecular orbital energy gap (E_g), total energy, density of states (DOS), radial distribution functions (RDFs), order parameter (R) to analyze the segregation phenomena of Cu and H atoms and the number of bonds between Cu-Cu, Cu-H and H−H binary interactions in CuH NPs. In order to conduct structural analysis, we also developed programs in R language (discussed in the next section) to analyze the number of

* Corresponding author.
** Corresponding author at: Computer Science Department, Indiana University, Bloomington, 47405, IN, USA.
E-mail addresses: hakurban@gmail.com (H. Kurban), mkurbanphys@gmail.com (M. Kurban).

https://doi.org/10.1016/j.mtcomm.2019.100648
Received 1 September 2019; Received in revised form 15 September 2019
Available online 26 September 2019
2352-4928/ © 2019 Elsevier Ltd. All rights reserved.

bonds, segregation phenomena, and RDF.

2. The method of calculations

The structural analysis and electronic structure of CuH NPs have been investigated using DFTB implemented in DFTB + code [29] with the hyb-0-2 [30,31] set of Slater Koster parameters. The DFTB formalism contains two major contributions (see Eq. (1)). These contributions correspond to the Hamilton and overlap matrix elements, and the repulsive potentials [32]. The basic idea of the DFTB formalism is to perform the second order expansion of the Kohn-Sham (KS) DFT total energy functional around a reference electronic density (ρ_0),

$$E^{total} = E^0[\rho_0] + E^1[\rho_0, \delta\rho] + E^2[\rho, (\delta\rho)^2] \quad (1)$$

where ρ_0 is the sum of neutral atomic densities. The first term in Eq. (1) is a Kohn-Sham effective Hamiltonian which is defined as

$$E^0[\rho_0] = \hat{H}_0 = \langle \eta_\mu | \hat{H}[\rho_0] | \eta_\nu \rangle \quad (2)$$

and the second term is the energy due to charge fluctuations

$$E^1[\rho_0, \delta\rho] = \frac{1}{2}\hat{S}_{\mu\nu}\sum_X (\gamma_{AX} + \gamma_{BX})\Delta q_X \quad (3)$$

where $\hat{S}_{\mu\nu} = \langle \eta_\mu | \eta_\nu \rangle$ is the overlap matrix elements. For the first two terms, the Hamiltonian and overlap of atomic orbitals are precalculated and stored as well as a self-consistent charge (SCC) procedure is used in the SCC-DFTB approach to self consistently due to the dependence of the DFTB Hamiltonian on the atomic charge. The third term is the repulsive potential which is approximated as a sum of two-center repulsions,

$$E^2[\rho, (\delta\rho)^2] = \frac{1}{2}\sum_{A,B} V_{AB}(|\overrightarrow{R_A} - \overrightarrow{R_B}|) \quad (4)$$

with pair potentials which depend on the respective atom types and the interatomic distance $R_{AB} = \overrightarrow{R_A} - \overrightarrow{R_B}$. We do not explain the procedure of DFTB calculations in detail because there currently exist several studies available with detailed descriptions of theoretical aspects and performance of the DFTB approach, as well as advances in theoretical development and application [33–36].

The initial structures of some of CuH NPs from $n = 204$ to 2418 atoms are indicated in Fig. 1. All of the CuH NP models were carved from bulk $60 \times 60 \times 60$ supercell of hexagonal crystal structure (wurtzite, space group $P6_3mc$) with the unit cell lattice constants a = 2.74 Å and c = 4.39 Å observed in experiments [37,38]. The chemical arrangement of Cu and H concentrations was chosen as $x = 0.50$ ($Cu_{1-x}H_x$). All calculations have been performed at constant volume.

To make the program more accessible to non-computational scientists, we have designed and implemented programs to simplify structural analysis. These includes functions to analyze the number of bonds, segregation phenomena, and RDF of CuH NPs based on the size. We also have made the codes of the properties mentioned above open source freely available online (https://github.com/hasankurban/Structural-Analysis-NanoParticles). Additionally, these programs include high resolution visualizations to plot data, though our intent is broader than the scope of the work in this paper.

We have chosen R—itself an open source programming language—that is among the most ubiquitously used platforms (R includes both an interactive environment and IDE-like versions), and is found in

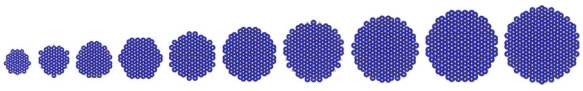

Fig. 1. Initial structures of some CuH spherical nanoparticles from $n = 204$ to 2418 atoms. (Cu is blue, H is yellow).

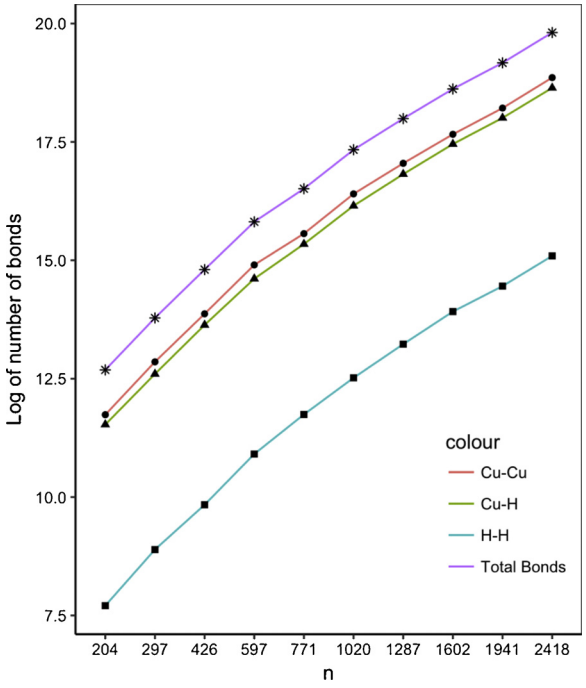

Fig. 2. Variation of number of bonds of binary Cu-Cu, Cu-H and H—H interactions based on the size of CuH nanoparticles.

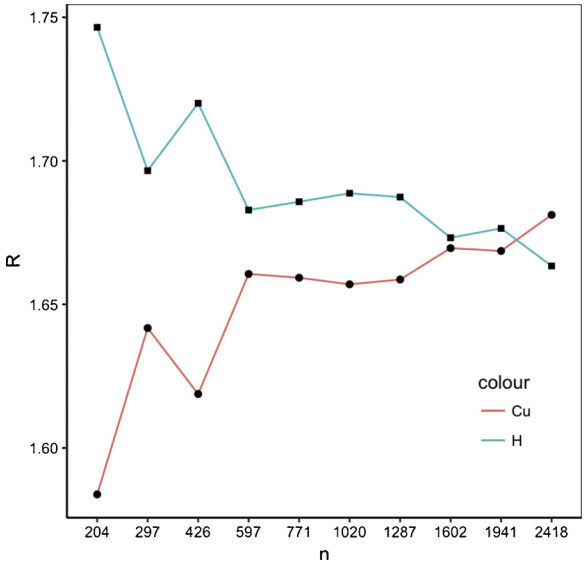

Fig. 3. Size dependence of the order parameter of Cu and H atoms in the CuH nanoparticles.

virtually all computational and data science analyses and has become one of the most common scientific computational tools. It is our belief that for these reasons, R is both a necessary and excellent too for the material science community if material science is to stay current with the general tendency to include computation as part of any scientist's skill set. To address the likely problem many, if not most, material scientists are not programmers, we have carefully designed the tools to be to be easily used and, for those who can, placed in GitHub, to tailor the code for their own needs. In the near future our plan is to the software as a web service to further simplify usage.

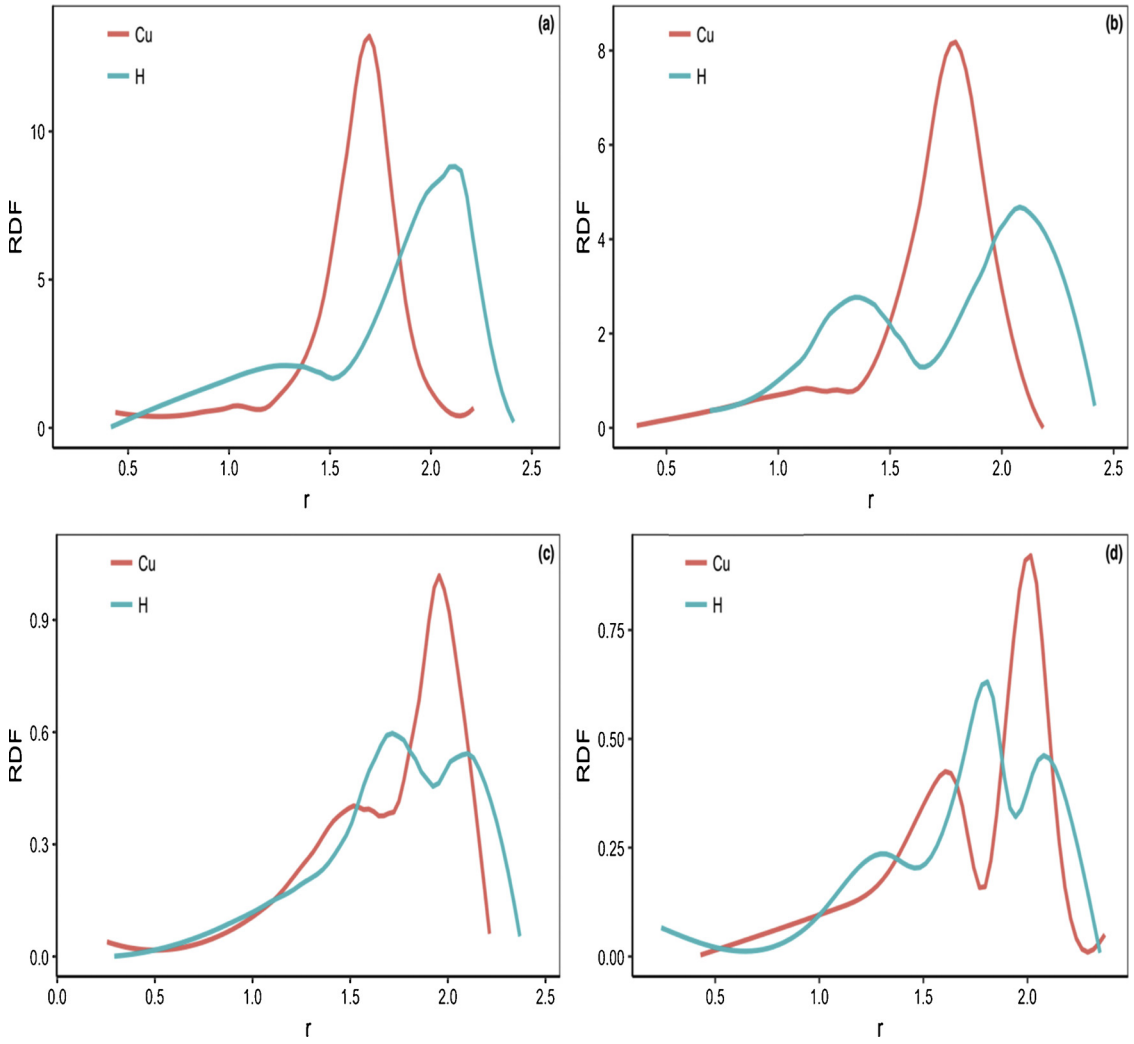

Fig. 4. Radial distribution function of CuH nanoparticles with (a) n = 204, (b) 297, (c) 1941 and (d) 2418 atoms.

3. Results and discussions

3.1. Structural analysis

The number of the nearest neighbor contacts (n_{ij}), that is the number of bonds, is generally adopted to distinguish the degree of packing, which is an important property of NPs. The number n_{ij} [39] for the NPs is given by

$$n_{ij} = \sum_{i<j} \delta_{ij} \tag{5}$$

where $\delta_{ij} = \begin{cases} 1, & r_{ij} \le 1.2r_{ij}^{(0)} \\ 0, & r_{ij} > 1.2r_{ij}^{(0)} \end{cases}$ i, j= Cu or H, r_{ij} is the distance between atom i and j and $r_{ij}^{(0)}$ is a nearest neighbor criterion derived by fitting the experimental data [40]. Thus, the number of bonds is used to analyze the atomic distribution of Cu and H atoms in the CuH NPs. We used Algorithm I for this process in which the input parameters are the data set D, which is centered at the origin, and the nearest neighbor criterion $r_{ij}^{(0)}$ which are pre-calculated and show the smallest distance between binary interactions (line 2). After calculating new r_{ij} values, the algorithm compares them with the input values $r_{ij}^{(0)}$ as shown in line 5 and returns the nearest number contact counts for each binary interaction.

Algorithm 1 Nearest Neighbor Contacts over D

1: %% D is centered at the origin
2: **INPUT** data D, nearest neighbor criterion $r_{ij}^{(0)}$
3: **OUTPUT** Nearest Neighbor Contacts r_{ij}
4: %% i, j: element type, i.e., Cu, H
5: $r_{ij} = \sum_{i<j} \delta_{ij}$ where

$$\delta_{ij} = \begin{cases} 1, & \text{if } r_{ij} \leqslant 1.2r_{ij}^{(0)} \\ 0, & \text{otherwise } r_{ij} > 1.2r_{ij}^{(0)} \end{cases}$$

Fig. 2 shows the numbers of bonds in CuH NPs with different sizes ranging from 204 to 2418 atoms. From the curve of CuH NPs shown in Fig. 2, it is clear that the number of Cu-Cu, Cu-H and H−H (H_2) bonds increase gradually with increased the size of CuH NPs. Furthermore, the number of Cu-H bonds is relatively smaller than that of Cu-Cu, while H−H bonds are the smallest. This means that Cu atoms tend to form more bonds with Cu atoms: that H−H tend to scatter on the surface can likewise be inferred. Moreover, the number of Cu-Cu bonds is larger than that of Cu-H and H−H bonds; therefore, it appears that Cu atoms have a greater preference for Cu atoms than for H atoms. When it comes to geometrical shapes, there is a sharp increase in the number of bonds of the CuH nanoparticle including 597 atoms with hexagon shape.

One of the major problems of some materials [41] is the formation of a stable structure for getting high-efficiency devices. The distribution

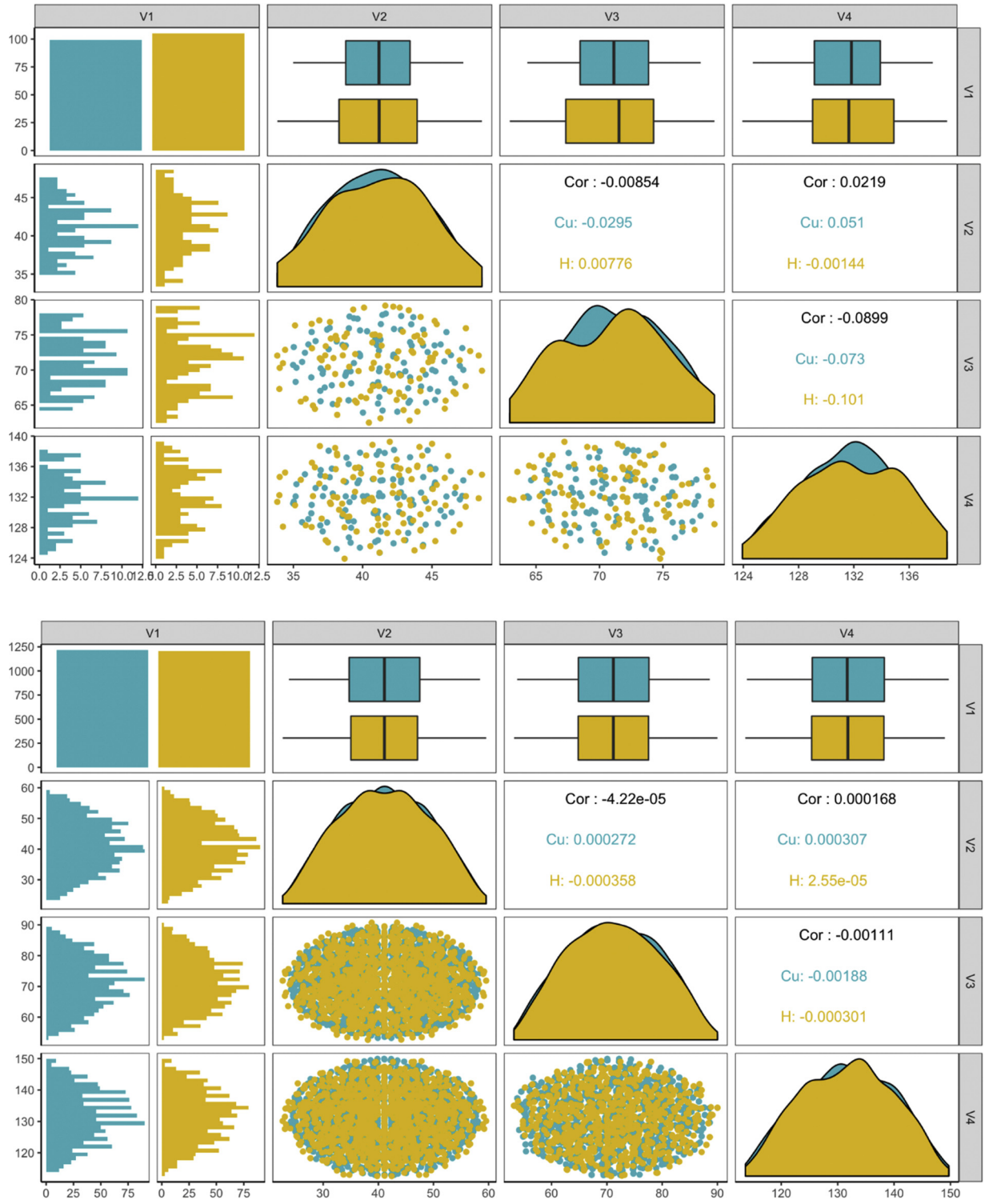

Fig. 5. Structural analysis of the data sets with 204 and 2418 atoms.

of atoms in crystalline structures is, in general, uniform and homogeneous [42]. Thus, the order parameter (R_{T_i}) is calculated to determine the stable structure in NPs by analyzing the distribution of the different types of atoms [39,43]. R_{T_i} is identified by the average distance of a type T_i atoms in accordance with the center of a NP,

$$R_{T_i} = \frac{1}{n_{T_i}} \sum_{i=1}^{n_{T_i}} r_i \tag{6}$$

where n_{T_i} is the number T_i type atoms in the ternary ABC NPs, and r_i is the distance of the atoms to the coordinate center of the NP. If an ε distance from center of NP to a reference point is defined to show the location of atoms; if $R_{T_i} < \varepsilon_{min}$ (a "small" value), it means that the T_i type atoms are at the center, and if $R_{T_i} > \varepsilon_{max}$ (a "large" value), it means that the T_i type atoms are at the surface region of NP. If neither is true, *i.e.*, if $\varepsilon_{min} \leq R_{T_i} \leq \varepsilon_{max}$ (a "medium" value), it means a well-mixed NP. The R_{T_i} of each atom type is analyzed using algorithm 2. The algorithm takes D, data set (Line 2), as an input and calculates the order parameter values R_{T_i} as shown in line 9 where n_{T_i} represents the number of

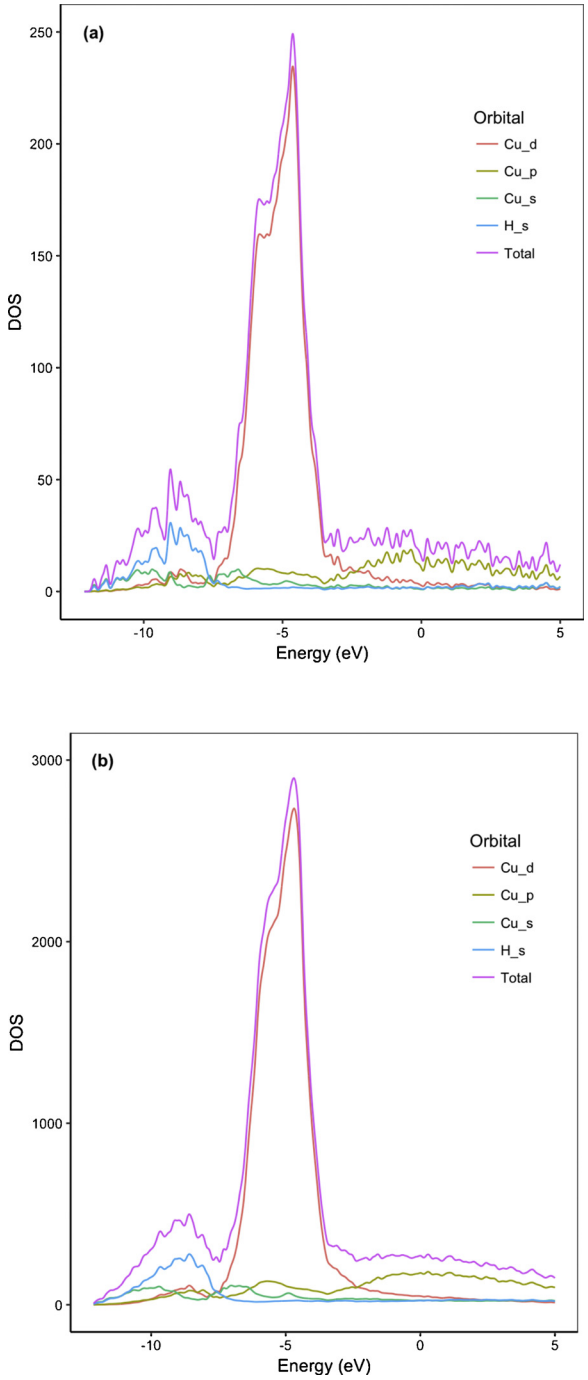

Fig. 6. The partial and total density of states (DOS) of CuH nanoparticles with (a) $n = 204$ and (b) 2418 atoms.

atoms for atom type T_i and x_j, y_j and z_j are the coordinates of the atom j.

Algorithm 2 Order Parameter over D

```
%% D is centered at the origin
INPUT data D
OUTPUT Order parameter R_T
%% T_i: element type, T_i ⊆ D, i.e., T_1 = Cu, T_2 = H
for T_i ∈ D do
    %% n_{T_i}: number of atoms of type T_i
    %% R_{T_i}: order parameter for element type T_i
    %% x_j, y_j, z_j: coordinates of the atom j
    R_{T_i} = (1/n_{T_i}) Σ_{j=1}^{n_{T_i}} sqrt(x_j^2 + y_j^2 + z_j^2)
end for
```

Fig. 3 shows the behavior of R of Cu and H atoms in terms of the NP size. The segregation behavior of atoms in the Cu-H NPs is performed using the order parameter. The segregation of Cu and H atoms show that Cu atoms tend to locate at the center, while H atoms tend to occupy the surface as a general trend. The segregation of H atoms to the surface is due to its lower cohesive energy. The R shows different characteristics with the increase of the size of CuH NPs. R_{Cu} values increase, and R_H decrease sharply for NPs with 297 and 597 atoms. R_{Cu} values decrease, and R_H increase for NP with 426 atoms. Later, there is a smooth decrease in R_{Cu} and a smooth increase in R_H for NPs with 771 and 1020 atoms, and then H atoms mainly grow on the surface, while Cu atoms mainly tend to co-locate at the center.

The Radial Distribution Function (RDF) is an important structural characteristic that defines the probability of finding a particle at a distance r from another tagged particle. The RDF is mathematically defined as Line 16 $g_{(r_i)} = n_{(r_i)}/(|\Delta| \times V_s \times V_d)$ where $n_{(r_i)}$ is the mean number of atoms in a shell of width dr at distance r_i, $|\Delta|$ represents total atom number and V_s is the volume of the spherical shell and V_d is the mean atom density. Algorithm III describes the RDF over D and takes three inputs: data set D, a distance vector $\boldsymbol{r}$, and a distance vector dr that denotes the thickness of a spherical shell.

Algorithm 3 Radial Distribution Function (RDF) over D

```
%% dr: thickness of a spherical shell & dr ∈ (0, 1)
%% r can be given to the program as an input or
%% randomly constructed while program executes.
%% D is centered at the origin, O: origin, x ∈ D
INPUT data D, distance vector r, distance dr
OUTPUT g(r): RDF values for the particles in D
for r_i ∈ r do
    %% n(r_i): mean number of atoms in a shell of
    %% width dr at distance r_i
    n(r_i) =|D_i| ∋ D_i ⊆ D & r_i ⩽ d(x, O) ⩽ r_i + dr
    %% V_s: Volume of the spherical shell.
    V_s = 4πr_i^2 dr
    %% V_d: the mean atom density.
    V_d =|D|/(4/3 πr_i^3)
    %% g(r_i): RDF value for r_i
    g(r_i) = n(r_i)/ (|D| ×V_s × V_d)
end for
```

Fig. 4 shows the RDF Cu-Cu, Cu-H and H-H binary interactions in CuH NPs with (a) $n = 204$ and (b) 297, (c) 1941 and (d) 2418 atoms. The RDFs are calculated for each atomic pair of optimized CuH NPs. Cu-H has a narrower and higher distribution than H-H interactions. When it comes to size dependence, the peaks for both pairs also decrease with increasing NP size. Moreover, the fluctuations of obvious peaks in the RDF also increase with raising the NP size.

Fig. 5 demonstrates statistical properties of each variable and bilateral relationships between the variables. To keep the discussion simple, we only show the results for the data sets which have smallest and largest atom numbers; 204 and 2418. Each of the ten data sets used

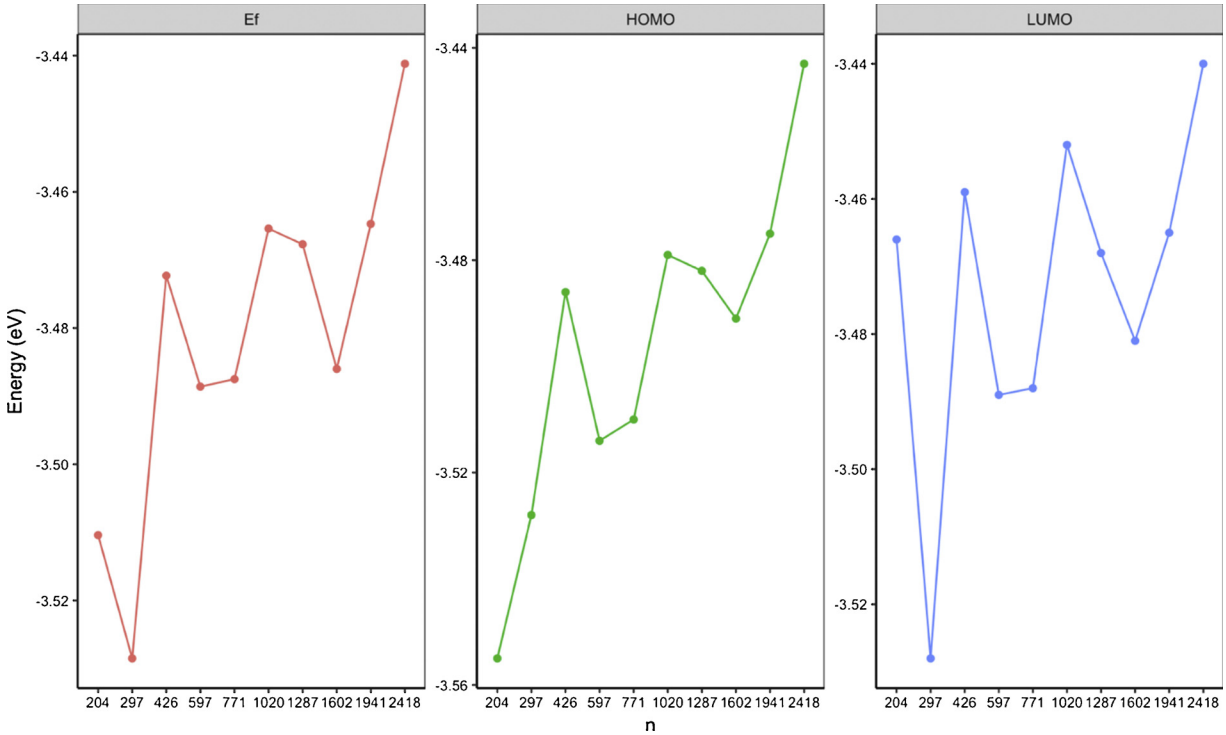

Fig. 7. HOMO, LUMO and Fermi energies of CuH nanoparticles in terms of size.

in this study is a 4-dimensional data set with different atom numbers. The first variable (V1) is categorical and has information about element type and the rest of the variables are continuous. Fig. 5 shows that there is no linear relationship between the variables, and each variable is normally distributed. Moreover, the distribution of the atoms between elements appears balanced.

3.2. Electronic structure

To obtain detailed information on electronic states in CuH NPs, we report in this study the results of the electronic partial and total DOS of different sizes as seen in Fig. 6(a, b). The density of localized states increases concomitantly with the size of CuH NP where the greatest contribution is coming from the *d*-orbital of Cu atoms. The fluctuations considerably disappear based on the increase in the size of CuH NPs. The density of localized states has a sharply increasing tendency in the region of between -8 and -2 eV. The DOS analysis also indicates that CuH NPs has no energy gap, so, all the NPs show metallic character. According to experimental observations, hexagonal bulk CuH shows semiconductor character; while its NP shows metallic character. Thus, the predicted results in this study are compatible with experimental data [44]. There are a decrease and an increase in HOMO, LUMO and Fermi energy with increasing the size of NPs. The HOMO value for the NP with 204 atoms (the smallest one) is -3.55 eV wide, *i.e.*, about 0.11 eV greater than the biggest NP with 2418 atoms. The NP with 2418 atoms has the lowest HOMO value (-3.44 eV) and thus it is less reactive due to the smallest HOMO value, while being more stable than the other CuH NPs (see Fig. 7). Fermi energy levels are found to be the bottom of the valence band and closer to the LUMO energy levels.

4. Conclusion

In this study, we have investigated the size dependence of structural and electronic properties of CuH nanoparticles containing from 204 to 2418 atoms, using the density functional tight binding (DFTB) approach. To perform structural analysis, we designed, implemented, and tested R code which can be easily used by non-programmers to analyze the number of bonds, segregation phenomena, and RDFs of binary interactions in CuH NPs. From the results of our calculations, we found that the number of bonds Cu-Cu is bigger than that of Cu-H while H_2 bonds are the smallest. Thus, the ability of Cu atoms to absorb large amounts of H is more than H_2. The increase in the size of the NPs contributes to the stabilization because of the enhanced strength of H−H bonding. The segregation of Cu and H atoms show that Cu atoms tend to co-locate at the center, while H atoms tend to reside on the surface. The size dependence of the HOMO, LUMO, and Fermi energy levels becomes greater when the size of NP decreases. The decrease in the HOMO levels contributes to the stabilization of CuH NP. From experimental data, CuH in wurtzite bulk form shows semiconductor character, whereas, interestingly, CuH NPs shows metallic character. From the density of state (DOS) analysis, CuH NPs shows a metallic character which is compatible with experimental data and is caused by an increase in the size of CuH NP. These results will provide insight into the storage of hydrogen based on the CuH NPs.

Declaration of Competing Interest

We have no conflict of interest to declare.

Acknowledgments

The numerical calculations were also partially performed at TUBITAK ULAKBIM, High Performance and Grid Computing Centre (TRUBA resources), Turkey.

References

[1] A.C.R. Würtz, Hebd. Seances, Acad. Sci. 18 (1844) 702.
[2] L. Burzyńska, J. Stoch, Z. Zembura, Solid State Ion. 38 (1990) 179.
[3] L. Burzyńska, J. Karp, Z. Zembura, Solid State Ion. 73 (1994) 35.
[4] A. Vaškelis, R. Juškėnas, Jačiauskienė, J. Electrochim. Acta 43 (1998) 1061.
[5] A.J. Elliott, B. Sakakini, J. Tabatabaei, K.C. Waugh, F.W. Zemicael, R.A. Hadden, J. Chem. Soc. Faraday Trans. 91 (1995) 3659.
[6] N.P. Fitzsimons, W. Jones, P.J. Herley, Catal. Lett. 15 (1992) 83–94.
[7] H. Tanaka, Y. Yamaguchi, S.-I. Sumida, M. Kuroboshi, M. Mochizuki, S.J. Torii, J. Chem. Soc. Perkin Trans. I 1 (1999) 3463.

[8] S. Rendler, M. Oestreich, Angew. Chem. Int. Ed. 46 (2007) 498.
[9] C. Deutsch, N. Krause, B.H. Lipshutz, Chem. Rev. 108 (2008) 2916.
[10] M.R. Churchill, S.A. Bezman, J.A. Osborn, J. Wormald, Inorg. Chem. 11 (1972) 1818.
[11] W. Haoxuan, C.Y. Jeff ;rey, L.B. Stephen, J. Am. Chem. Soc. 139 (2017) 842.
[12] Z. Yujing, S.B. Jeff ;rey, L.B. Stephen, J. Am. Chem. Soc. 139 (2017) 8126.
[13] L. Gang, Y.L. Richard, Y. Yang, F. Cheng, S.L. Daniel, L.B. Stephen, L.J. Peng, Am. Chem. Soc. 139 (2017) 16548.
[14] V. Antonov, Alloys J. Compd. 330 (2002) 110.
[15] S.M. Filipek, J. Adv. Sci. 19 (2007) 1.
[16] M. Tkacz, R. Burtovyy, Alloys J. Compd. 404 (2005) 368.
[17] C.L. Wang, H. Zhang, J.H. Zhang, M. Li, H.Z. J Sun, B. Yan, J. Phys. Chem. C 111 (2007) 2465.
[18] P. Yang, S. Tretiak, A.E. Masunov, S. Ivanov, J. Chem. Phys. 129 (7) (2008) 74709.
[19] M. Kurban, J. Alloys Compd. 791 (2019) 1159.
[20] M. Kurban, Turk. J. Phys. 42 (2018) 443.
[21] M. Kurban, S. Erkoç, J. Comp. Theor. Nanosci. 12 (2015) 2605.
[22] I.L. Soroka, N.V. Tarakina, P.A. Korzhavyi, V. Stepanenko, M. Jonsson, CrystEngComm 15 (2013) 8450.
[23] R.S. Dhayal, W.E. van Zyl, C.W. Liu, Dalton Trans. 48 (2019) 3531.
[24] A. Pavel, I.L. Korzhavyia, E.I. Soroka, C.L. Isaev, J. Börje, PNAS 109 (2012) 86.
[25] Y. Li, P.A. Korzhavyi, Dalton Trans. 46 (2017) 529.
[26] V. Maurya, G. Sharma, U. Paliwal, K.B. Joshi, Comput. Mater. Sci. 150 (2018) 329.
[27] N.V. Ilawe, M.B. Oviedo, B.M. Wong, J. Mater. Chem. C 6 (2018) 5857.
[28] N.V. Ilawe, M.B. Oviedo, B.M. Wong, J. Chem. Theory Comput. 13 (2017) 3442.
[29] B. Aradi, B. Hourahine, T. Frauenheim, J. Phys. Chem. A 111 (2007) 5678.
[30] Z. Hajnal, Th. Frauenheim, C. González, J. Ortega, R. Pérez, F. Flores, Appl. Surf. Sci. 212–213 (2003) 861.
[31] Z. Hajnal, R. Scholz, S. Sanna, Th. Frauenheim, Appl. Surf. Sci. 234 (2004) 173.
[32] M. Gaus, A. Goez, M. Elstner, J. Chem. Theory Comput. 9 (2013) 1.
[33] M. Shahidul, R. Islam Pierre-Nicholas, J. Chem. Theory Comput. 87 (2012) 2412.
[34] M.A. Addicoat, R. Stefanovic, G.B. Webber, R. Atkin, A.J. Page, J. Chem. Theory Comput. 10 (10) (2014) 4633.
[35] T. Frauenheim, G. Seifert, M. Elsterner, Z. Hajnal, G. Jungnickel, D. Porezag, S. Suhai, R. Scholz, Phys. Status Solidi B 217 (2000) 41.
[36] T. Frauenheim, G. Seifert, M. Elstner, T. Niehaus, C. Kohler, M. Amkreutz, M. Sternberg, Z. Hajnal, A.D. Carlo, S. Suhai, J. Phys. Condens. Matter 14 (2002) 3015.
[37] R. Burtovyy, M. Tkacz, Solid State Commun. 131 (2004) 169.
[38] R. Burtovyy, D. Włosewicz, A. Czopnik, M. Tkacz, Thermochim. Acta 400 (2003) 121.
[39] X. Wu, Z. Wei, Q. Liu, T. Pang, G. Wu, J. Alloys Compd. 687 (2016) 115.
[40] https://cccbdb.nist.gov/exp2x.asp?casno=13517005&charge=0.
[41] T.C. Yu, R.F. Brebrick, J. Phase Equilibria Diffus. 13 (1992) 476.
[42] C. Lu, Y. Cheng, Q. Pan, X. Tao, B. Yang, G. Ye, Sci. Rep. 6 (2016) 19870.
[43] M. Kurban, O.B. Malcıoğlu, Ş. Erkoç, Chem. Phys. 464 (2016) 40.
[44] C.M. Lousada, R.M.F. Fernandes, N.V. Tarakina, I.L. Soroka, Dalton Trans. 46 (2017) 6533.